Palaeogeography, Palaeoclimatology, Palaeoecology 463 (2016) 168–179

Contents lists available at ScienceDirect

Palaeogeography, Palaeoclimatology, Palaeoecology

journal homepage: www.elsevier.com/locate/palaeo

Bone diagenesis variability among multiple burial phases at Al Khiday (Sudan) investigated by ATR-FTIR spectroscopy

Gregorio Dal Sasso [a,*], Matthieu Lebon [b], Ivana Angelini [c], Lara Maritan [a], Donatella Usai [d], Gilberto Artioli [a]

[a] Dipartimento di Geoscienze, Università degli Studi di Padova, Via G. Gradenigo 6, 35131 Padova, Italy
[b] Unité Mixte de Recherche 7194 "Histoire Naturelle de l'Homme Préhistorique", Centre National de la Recherche Scientifique, Muséum National d'Histoire Naturelle, Sorbonne Universités, 17 place du Trocadéro, F-75016 Paris, France
[c] Dipartimento dei Beni Culturali: archeologia, storia dell'arte del cinema e della musica, Università degli Studi di Padova, Piazza Capitaniato 7, 35139 Padova, Italy
[d] Centro Studi Sudanesi e Sub-Sahariani (CSSeS), Strada Canizzano 128/d, 31100 Treviso, Italy

ARTICLE INFO

Article history:
Received 20 May 2016
Received in revised form 3 October 2016
Accepted 6 October 2016
Available online 8 October 2016

Keywords:
Fossil bone
Diagenesis
Fourier transform infrared spectroscopy
Bioapatite
Early Holocene palaeoenvironment
Sudan

ABSTRACT

In this study the diagenetic pathways of archaeological human bones are investigated through Fourier transform infrared spectroscopy in attenuated total reflection mode (ATR-FTIR). Archaeological excavations at Al Khiday (16-D-4 site, Khartoum, Sudan) revealed a multi-stratified cemetery with distinct burial phases, chronologically attributed to different periods spanning from the Early Holocene to the beginning of the 1st millennium CE. ATR-FTIR measurements are carried out on a set of 56 bone samples, representative of each burial phase. Parameters related to collagen content and to bioapatite crystallinity and structural carbonate are calculated from infrared spectra in order to monitor the types and extent of diagenetic alteration, to assess the preservation state of bones and to define the alteration processes occurring during burial. A new method is here developed to quantify the amount of secondary calcite and to remove its contribution to the infrared spectrum, when interfering with the signal of structural carbonate from bioapatite.

Considering the wide span of time covered by the archaeological record, the variability of bones alteration among burial phases is related to the climatic changes occurring in central Sudan during the Holocene. The more humid environment occurring in the Early Holocene, characterised by higher precipitation rates, seasonal swamps and palaeo-lakes, progressively changed towards drier conditions until the current arid climate of the Sub-Saharan belt. The change of palaeoenvironmental and local burial conditions over time differently influenced the types and extent of diagenetic processes affecting bones during burial.

In this research are also discussed advantages and disadvantages of ATR-FTIR spectroscopy with respect to the more established FTIR spectroscopy in transmission mode.

1. Introduction

Human bones are frequently found within the archaeological record and are studied at different levels in order to retrieve valuable information for anthropological, cultural and palaeoenvironmental studies. Bone is a composite material with a complex structure described in terms of hierarchical levels of organization (Weiner and Wagner, 1998), constituted by the association of an organic matrix (mainly type-I collagen) and a mineral phase. The latter is constituted by nanocrystals of bioapatite, with a composition resembling that of hydroxyapatite ($Ca_{10}(PO_4)_6(OH)_2$) but considerably departing from stoichiometry, as a number of elements enter the structure in minor and trace quantity and ionic substitutions occur (Gómez-Morales et al., 2013; Elliot, 2002; LeGeros, 1981). After the death of the individual, bones undergo several taphonomic and diagenetic processes, mainly influenced by environmental and burial conditions, that cause the alteration of both their organic and mineral constituents at different extent. Collagen deterioration, microbiological alteration, bioapatite dissolution and recrystallization, ions depletion or uptake and secondary mineral phases precipitation can occur (Lee-Thorp, 2008; Hedges, 2002; Nielsen-Marsh and Hedges, 2000; Smith et al., 2007; Sponheimer and Lee-Thorp, 1999; Weiner, 2010). The study of bone diagenesis for a specific site aims to understand how, by which way and at which extent these processes have altered archaeological bones; moreover, if subsequent studies are addressing the recovery of the pristine chemical composition or isotopic signature of bones, the study of diagenetic alteration may contribute to assess the reliability of retrieved information.

This research investigates the diagenetic alteration of human bones from the archaeological site 16-D-4 at Al Khiday (Khartoum, Sudan), where a multi-stratified cemetery was excavated, revealing four

* Corresponding author.
E-mail address: gregorio.dalsasso@unipd.it (G. Dal Sasso).

http://dx.doi.org/10.1016/j.palaeo.2016.10.005
0031-0182/

different burial phases, covering a wide span of time, from the pre-Mesolithic to the Meroitic (Dal Sasso et al., 2014; Jakob, 2014; Usai et al., 2010; Usai et al., 2014), namely from the early Holocene to the early 1st millennium CE. Since, profound climatic changes occurred during the Holocene in North Africa, from humid environment towards drier conditions more similar to the current arid climate of the Sub-Saharan belt (Castaneda et al., 2009; Clarke et al., 2015; Gasse, 2000; Gatto and Zerboni, 2015; Hoelzmann et al., 2001; Kröpelin et al., 2008; Nicoll, 2004; Talbot et al., 2007; Zerboni, 2013; Williams et al., 2015), this case study investigates a set of bone samples that have been buried in the same site but at different periods, thus experiencing different environmental conditions. Moreover, since all burial phases share the similar ritual practise of burying the dead in pits, presumably shortly or even immediately after death, environmental and local burial conditions play a major role in determining different types of diagenetic alteration.

These bones were analysed through Fourier transform infrared spectroscopy (FTIR). This analytical approach is widely used in bone diagenesis studies (Lebon et al., 2008, 2010; Nielsen-Marsh and Hedges, 2000; Reiche et al., 2010; Roche et al., 2010; Smith et al., 2007; Trueman et al., 2004; Weiner, 2010) as it requires a low amount of material (1 mg) and it is sensitive in investigating both the mineral and the organic phase. Additionally, the fast and nearly inexpensive analytical procedure enables one to investigate a large set of samples. A FTIR spectrum shows which fraction of the incident infrared radiation is absorbed by the sample at a particular wavelength, thus providing information on molecular bonds and their chemical environment. Qualitative and semi-quantitative analyses can be performed in order to investigate the nature as well as the atomic order/disorder of mineral and organic matter in the analysed samples. Therefore, FTIR spectroscopy can provide valuable information on the preservation state as well as on structural and chemical properties of archaeological bones (Grunenwald et al., 2014; Lebon et al., 2010; Weiner and Bar-Yosef, 1990; Weiner, 2010).

Several analytical techniques coupled with FTIR spectroscopy are currently applied to material characterisation, requiring different sample preparation methods. While the traditional transmission FTIR mode, performed on pellets prepared with potassium bromide (KBr), is extensively used to study bone material, only recently Attenuated Total Reflection FTIR (ATR-FTIR) mode has been applied to provide both qualitative and quantitative information on fossil bone composition and to investigate bone diagenesis (Beasley et al., 2014; Hollund et al., 2012; Lebon et al., 2014, 2016; Salesse et al., 2014). The main advantage of applying FTIR spectroscopy in ATR mode rather than in transmission mode is the minimal sample preparation that is required, implying faster analysis and reducing the influence of sample preparation on the measurements. In fact, the use of different protocols to prepare KBr pellets and even the same preparation procedure performed by different operators can induce at least minimal differences in FTIR spectrum, which however heavily affect the determination of diagenetic parameters calculated on the basis of peaks intensity ratio (Asscher et al., 2011a, 2011b; Surovell and Stiner, 2001). Moreover, KBr is hygroscopic, thus an accurate and time consuming sample preparation is required in order to reduce at minimum the effects of atmospheric moisture on the acquired spectra; conversely, these effects are more easily removed when applying ATR-FTIR spectroscopy.

Taking into account all these aspects, this study aims to evaluate the preservation state of the archaeological bones found at Al Khiday by applying ATR-FTIR spectroscopy, and to define the diagenetic processes affecting bones, considering the changes of climatic and environmental conditions during burial.

2. FTIR spectroscopy of bone

When analysing bone material, major absorption bands of the organic matrix are located in the region from 1700 to 1300 cm^{-1}, where two peaks, at 1660 and 1550 cm^{-1} corresponding to the amide I and amide II vibrational bands, respectively, can be detected.

Bioapatite shows several absorption bands relative to phosphate and carbonate groups. In fact, among ionic substitutions in bioapatite crystal structure, carbonate substitution is the most significant (4–7 wt.%) and it is easily detectable by FTIR measurements.

Carbonate ions occur in the A and B crystallographic sites, substituting hydroxyl ions and phosphate ions, respectively, and are thought to stabilize the surface of apatite nanocrystals. The presence of ionic substitutions in the bioapatite structure influences the long-range atomic order of crystals and therefore it plays a major role in determining physical and chemical properties of bone mineral, such as solubility and crystal size (LeGeros, 1981; Wopenka and Pasteris, 2005). The occurrence of carbonate ions in the bioapatite structure produces, in the IR spectrum, bands referred to the $\nu_2(CO_3)$ and $\nu_3(CO_3)$ vibrational modes, detected in the range from 890 to 840 cm^{-1} and from 1600 to 1300 cm^{-1}, respectively (Fig. 1a, b). A more detailed distinction is between vibrational bands associated to carbonate ions occupying the A or B crystallographic site: it is almost accepted the attribution of the $\nu_3(CO_3)$ vibrational modes at ~1465 and ~1542 cm^{-1} to the A-type carbonate and at ~1462 and ~1415 cm^{-1} to the B-type carbonate, as well as the $\nu_2(CO_3)$ at ~880 cm^{-1} to the A-type carbonate and at ~872 cm^{-1} to the B-type carbonate (Rey et al., 2011). The possible presence of secondary calcite, frequently detected in archaeological bones as the result of secondary mineral phases precipitation in bone micro-porosity during diagenesis, can be monitored. In fact, while $\nu_2(CO_3)$ and $\nu_3(CO_3)$ vibrational modes overlap with those of carbonate ions in the bioapatite crystal structure, $\nu_4(CO_3)$ at 712 cm^{-1} is characteristic for calcite (Fig. 1c).

As for phosphate group, the strongest absorption bands correspond to $\nu_3(PO_4)$ and $\nu_4(PO_4)$ vibrational modes and range from 1200 to 900 cm^{-1} and from 700 to 500 cm^{-1}, respectively; weaker bands, corresponding to $\nu_1(PO_4)$ and $\nu_2(PO_4)$ are at 962 cm^{-1} and 472 cm^{-1}, respectively (Rey et al., 2011) (Fig. 1a, b). The $\nu_4(PO_4)$ vibrational mode shows two bands at ~604 and ~565 cm^{-1} (and a shoulder at ~575 cm^{-1}), whose separation is correlated to atomic disorder and/or crystal size of bioapatite. Weiner and Bar-Yosef (1990) defined a crystallinity parameter, named infrared splitting factor (IRSF), calculated as the sum of peak intensities at 604 and 565 cm^{-1} divided by the intensity of the valley between them, thus quantifying the splitting extent of the two peaks. Since a good correlation between IRSF and the bioapatite crystal size, assessed by other analytical techniques (Piga et al., 2011; Stathopoulou et al., 2008; Trueman et al., 2004), was proved, the infrared splitting factor can be used as an effective parameter to monitor the bioapatite recrystallization degree. A bioapatite sample characterised by a more ordered crystal structure and larger crystals will show a higher value of IRSF than a less crystalline sample.

FTIR spectroscopy can provide simultaneous information on collagen preservation as well as on carbonate content and crystallinity of the bone mineral fraction. These parameters will be monitored thought the multiple burial phases at the Al Khiday site.

3. Materials and methods

3.1. Archaeological samples

The archaeological site 16-D-4 (or Al Khiday 2) is located in central Sudan near Khartoum, on the western bank of the White Nile, at 3.5 km from the river course and 22 km south from the confluence with the Blue Nile (Appendix A). Extensive archaeological excavation (Salvatori and Usai, 2009; Salvatori et al., 2011, 2014; Usai and Salvatori, 2005, 2007; Zerboni, 2011), carried out within the "El Salha archaeological project" since 2005, brought to light 203 graves belonging to at least three different burial phases: pre-Mesolithic, Neolithic and Meroitic (Dal Sasso et al., 2014; Iacumin et al., 2016; Jakob, 2014; Usai et al., 2010, 2014). Since the early Holocene, the same area has been used as a burial ground in several periods.

The pre-Mesolithic phase (105 graves) is chronologically constrained by the Mesolithic use of the site, whose features, cutting in some cases

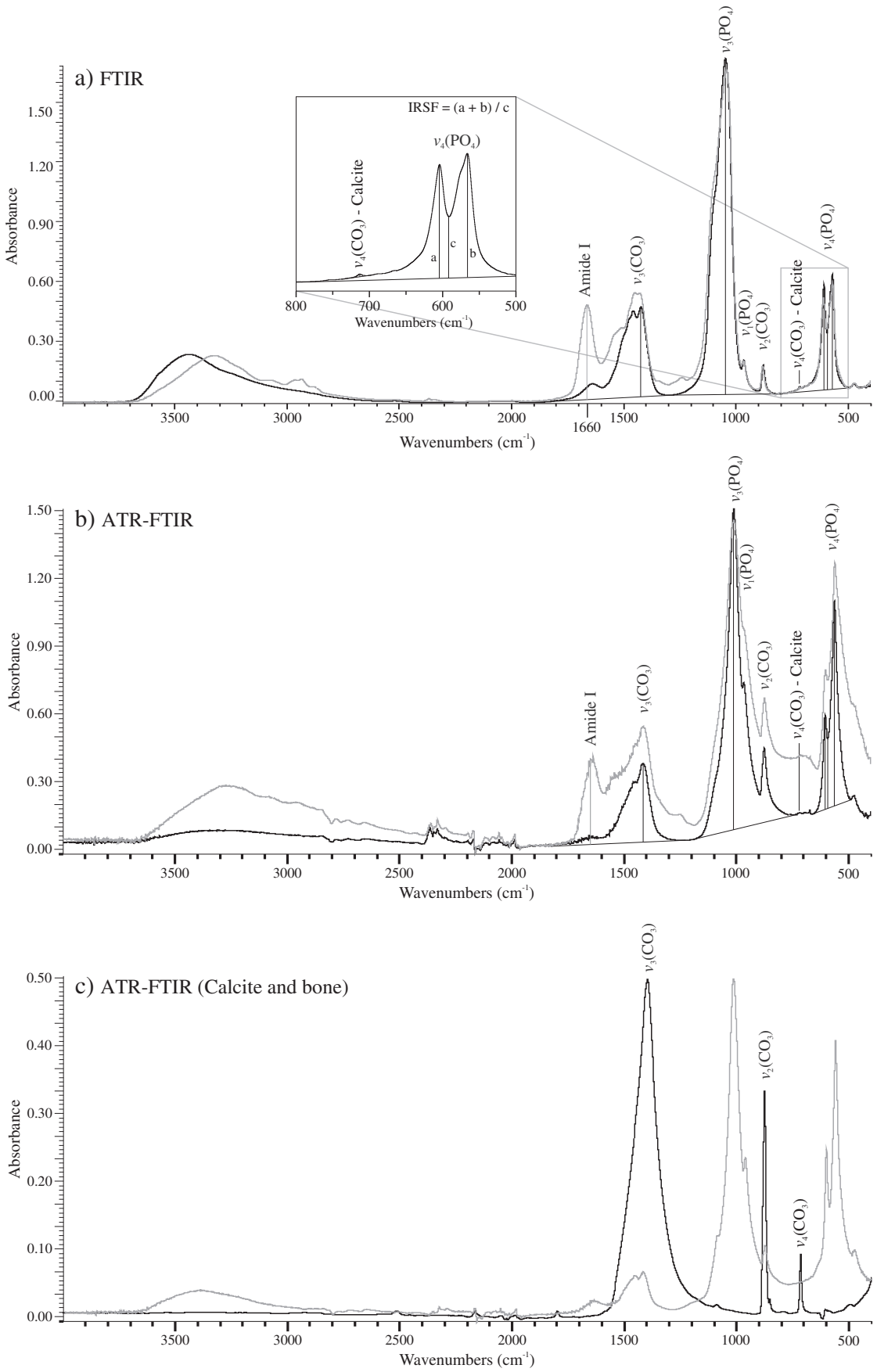

Fig. 1. FTIR spectra of an archaeological (black) bone sample (156F) and a modern (light grey) standard sample (2.5 wt.% of calcite, used for calibration curves), acquired in transmission (a) and ATR (b) modes, are reported. Bands are attributed to amide I, phosphate and carbonate vibrational modes. Peak intensities and baselines used to calculate Amide I/PO_4, CO_3/PO_4, Cal/PO_4 and IRSF parameters are shown. c. ATR-FTIR spectra of calcite (black) and bone (light grey – archaeological bone sample 50F).

the older burials, date to 6700–6300 cal. years BCE and provide a *terminus ante quem* for this burial phase (Salvatori et al., 2011; Salvatori, 2012; Usai et al., 2010). The site was subsequently used as a cemetery during the Neolithic period (30 graves; 4550–4250 cal. years BCE) and later on during the Meroitic period (42 graves, 50 cal. years BCE–250 cal. years CE) (Usai et al., 2010, 2014). The chronology of the burial phases was assessed on the basis of radiocarbon ages obtained on archaeological materials and soils sediments stratigraphically related to the graves (Salvatori et al., 2011; Usai et al., 2010; Williams et al., 2015). A possible fourth burial phase (19 graves, identified within the pre-Mesolithic group) was identified on the basis of both archaeological evidences and the macroscopic bone preservation state (Usai et al., 2010), coupled with histological analysis (Dal Sasso et al., 2014). However, the lack of grave goods and uncertainties on the relationship between graves and the archaeological stratigraphy make this burial phase of uncertain chronological attribution and it is here tentatively labelled as pre-Mesolithic-b.

In this research, 12 pre-Mesolithic, 3 pre-Mesolithic-b, 7 Neolithic and 6 Meroitic graves were selected as representative of the burial phases. From each grave a femur (F) and a humerus (H) were sampled, hence a total number of 56 bone samples were here analysed by ATR-FTIR spectroscopy (Table 1).

3.2. Standard samples for calibration curves

Significant variations among the burial phases, in terms of diagenetic alteration, were observed at the micro-scale level and secondary calcite was detected in pre-Mesolithic, pre-Mesolithic-b and Neolithic bone samples (Dal Sasso et al., 2014). The $\nu_2(CO_3)$ and $\nu_3(CO_3)$ vibrational bands of calcite overlap to those of structural carbonate of bioapatite, thus affecting the assessment of the preservation state of bioapatite by monitoring its carbonate content. Therefore, the following method has been developed in order to remove the contribution of calcite to the carbonate vibrational bands of spectra and to retrieve that of the structural carbonate of bioapatite.

A set of 8 standard samples were prepared adding ~1, 1.5, 2, 2.5, 5, 10, 15 and 20 wt.% (see Table 2 for exact wt.%) of calcium carbonate (Merck) to a deproteinated modern ox bone (bone was deproteinated by means of hydrazine hydrate 98% at room temperature for 2 h, then at ~40 °C for 48 h; finally bone mineral was rinsed once in 98% ethanol and in 100% ethanol for 3 times, then dried overnight at 45 °C). In this case, as archaeological bones are totally deprived of collagen (Usai et al., 2010), deproteinated bone was used as reference material. On the basis of results obtained by FTIR measurements, calibration curves were established in order to quantify secondary calcite in archaeological bones and decouple the overlapped contribution to the $\nu_3(CO_3)$ vibrational modes, generated by carbonate groups contained in calcite and in bioapatite. Measurement of standard samples was carried out by ATR-FTIR and FTIR in transmission mode; calibration curves obtained from the two different analytical techniques were compared in order to verify the reliability of results.

3.3. Sample preparation and measurement

Standard samples measured by ATR-FTIR spectroscopy were finely hand-ground and homogenized in an agate mortar. As for FTIR measurement in transmission mode using the KBr-pelleting technique, the following protocol has been applied in order to reduce at minimum the variations on spectra induced during sample preparation: about 10 mg of sample powder were dispersed in acetone and further ground for 30 min with an agate ball micro-mill, then 2.5 mg of ground sample were mixed with 1 g of KBr and homogenized in an agate mortar for 1 min. Transparent pellets (13 mm in diameter) were created by means of a vacuum hydraulic press, under 11 tons/cm^2 pressure for 2.5 min. Pellets were then dried in oven at 110 °C overnight before measurement.

Sample preparation of archaeological bones for ATR-FTIR measurement was minimal: the external surface of each sample, encrusted by soil sediments, was mechanically removed by means of low-speed micro-drill equipped with an abrasive point. Attention was paid in order to avoid over-heating of samples during the mechanical cleaning process. Then, samples were finely hand-ground in an agate mortar for about 1 min in order to homogenize their composition.

Spectra were collected with a Bruker Vector 22 spectrometer, equipped with an ATR diamond accessory (Specac Standard Golden Gate) for ATR-FTIR measurements; 64 scans for each spectrum were acquired, in the range 4000–400 cm^{-1}, with a spectral resolution of 2 cm^{-1}. Spectral analysis was performed using Omnic 9 software (Thermo Scientific).

The following parameters were calculated for each spectrum:

- parameter related to the carbonate content of bioapatite (**CO_3/PO_4**): calculated by dividing the intensity of the band at 1415 cm^{-1} ($\nu_3(CO_3)$ vibrational mode of B-type carbonate) by the peak intensity at 1035 cm^{-1} assigned to the $\nu_3(PO_4)$ vibrational mode (Grunenwald et al., 2014; Rink and Schwarcz, 1995); since B-type carbonate is much more abundant than A-type, CO_3/PO_4 parameter calculated here is assumed to produce reliable results in monitoring the carbonate content of bioapatite (LeGeros, 1981; Sponheimer and Lee-Thorp, 1999; Wopenka and Pasteris, 2005);
- parameter related to the amount of secondary calcite precipitated during diagenesis (**Cal/PO_4**): calculated by dividing the peak intensity at 712 cm^{-1} ($\nu_4(CO_3)$ vibrational mode characteristic for calcite) by the peak intensity at 1035 cm^{-1} of phosphate;
- infrared splitting factor (**IRSF**): calculated by dividing the sum of the peaks intensities at 604 and 565 cm^{-1} by the intensity of the valley between them (Weiner and Bar-Yosef, 1990); it is related to bioapatite crystallinity;
- collagen content parameter (**Amide I/PO_4**): calculated by dividing the peak intensity of the Amide I band at 1660 cm^{-1} by the peak intensity of the phosphate band at 1035 cm^{-1}; this parameter was determined in order to check the actual collagen degradation.

The baseline used to calculate band intensities was defined by two points calculated as the local minimum ranging in selected regions of the spectrum (Table 3).

4. Results

The relative standard deviation (RSD), calculated on repeated measurements of both standard and archaeological samples, is within 5% for IRSF, Cal/PO_4 and CO_3/PO_4 parameters. According to Lebon et al. (2016), a good reproducibility of ATR-FTIR measurements can be achieved by modulating the pressure on the ATR crystal in order to obtain a raw maximum absorbance below 1.

4.1. Calibration curves

4.1.1. ATR-FTIR

Results obtained from ATR-FTIR on the 8 standard samples (Table 2) show that the detection limit for calcite in bone-calcite mixture is ~ 2.5 wt.% since the 712 cm^{-1} band was not detected when analysing samples containing 1, 1.5 and 2 wt.% of calcite. Therefore, calibration curves were established considering just the results obtained from samples with 2.5, 5, 10, 15 and 20 wt.% of calcite. For each ATR-FTIR spectrum IRSF, Cal/PO_4 and CO_3/PO_4, were calculated.

An excellent correlation between Cal/PO_4 and calcite wt.% was observed (Fig. 2a) and the following linear correlation function was determined by linear regression:

$$[Cal/PO_4]_{ATR} = 0.0017[\text{calcite wt.}\%] - 0.0020 \quad (1)$$

Table 1
Diagenetic parameters calculated from the ART-FTIR spectrum of each sample and referring to: bone crystallinity (IRSF); secondary calcite content (Cal/PO_4); bioapatite carbonate content as calculated from spectra (CO_3/PO_4) and corrected for secondary calcite contribution (CO_3/PO_4-corr); collagen preservation (Amide I/PO_4). Calcite percentage (Calcite %) calculated from Cal/PO_4 values with Eq. (2) is also reported.

ATR-FTIR								
Burial phase	Grave number	Bone type	IRSF	Cal/PO_4	CO_3/PO_4	Amide I/PO_4	Calcite%	CO_3/PO_4-corr
Pre-Mesolithic	Grave 24	Femur	4.284	0.0117	0.2583	0.0192	8.0	0.2168
		Humerus	4.149	0.0115	0.2686	0.0255	7.9	0.2279
	Grave 55	Femur	4.492	0.0058	0.2521	0.0261	4.6	0.2315
		Humerus	4.161	0.0175	0.3002	0.0214	11.5	0.2378
	Grave 69	Femur	4.793	0.0284	0.2619	0.0165	17.9	0.1610
		Humerus	4.510	0.0271	0.3270	0.0185	17.1	0.2307
	Grave 88	Femur	4.063	0.0326	0.3922	0.0162	20.3	0.2765
		Humerus	4.037	0.0212	0.3386	0.0235	13.6	0.2634
	Grave 132	Femur	4.674	0.0030	0.2306	0.0288	2.9	0.2200
		Radius	4.247	0.0041	0.2468	0.0236	3.6	0.2323
	Grave 156	Femur	4.302	0.0051	0.2471	0.0232	4.2	0.2290
		Humerus	4.304	0.0048	0.2699	0.0243	4.0	0.2530
	Grave 157	Femur	4.273	0.0059	0.2840	0.0257	4.7	0.2629
		Humerus	4.112	0.0175	0.3438	0.0228	11.5	0.2816
	Grave 160	Femur	4.690	0.0383	0.3583	0.0179	23.7	0.2224
		Humerus	4.735	0.0241	0.2747	0.0176	15.4	0.1890
	Grave 170	Femur	5.218	0.0012	0.1584	0.0271		
		Humerus	5.113	0.0000	0.1785	0.0303		
	Grave 172	Femur	4.949	0.0124	0.2394	0.0213	8.5	0.1954
		Humerus	4.716	0.0037	0.2164	0.0281	3.3	0.2034
	Grave 174	Femur	4.742	0.0019	0.2052	0.0269		
		Humerus	4.859	0.0018	0.1868	0.0270		
	Grave 177	Femur	4.625	0.0005	0.2139	0.0270		
		Humerus	4.413	0.0027	0.2235	0.0258	2.7	0.2140
Pre-Mesolithic-b	Grave 31	Femur	5.160	0.0242	0.2329	0.0158	15.4	0.1467
		Humerus	5.016	0.0142	0.2360	0.0218	9.5	0.1856
	Grave 120	Femur	4.898	0.0120	0.2122	0.0215	8.2	0.1696
		Humerus	5.202	0.0092	0.1790	0.0194	6.6	0.1464
	Grave 128	Femur	4.804	0.0082	0.2379	0.0274	6.0	0.2088
		Humerus	4.914	0.0232	0.2970	0.0228	14.8	0.2145
Neolithic	Grave 3	Femur	4.838	0.0578	0.3660	0.0216	35.2	0.1604
		Humerus	5.133	0.0016	0.1553	0.0223		
	Grave 4	Femur	4.367	0.0050	0.2623	0.0337	4.1	0.2446
		Humerus	5.789	0.0038	0.1253	0.0196	3.4	0.1119
	Grave 103	Femur	4.614	0.0063	0.2332	0.0301	4.9	0.2107
		Humerus	4.508	0.0111	0.2533	0.0268	7.7	0.2139
	Grave 107	Femur	5.473	0.0069	0.1683	0.0229	5.2	0.1437
		Humerus	5.070	0.0197	0.2075	0.0197	12.8	0.1374
	Grave 158	Femur	4.160	0.0045	0.2490	0.0274	3.8	0.2331
		Humerus	5.628	0.0061	0.1364	0.0175	4.8	0.1146
	Grave 163	Femur	5.499	0.0027	0.1420	0.0228	2.8	0.1325
		Humerus	5.805	0.0026	0.1117	0.0169	2.7	0.1024
	Grave 164	Femur	5.673	0.0019	0.1178	0.0187		
		Humerus	5.554	0.0041	0.1234	0.0165	3.6	0.1088
Meroitic	Grave 50	Femur	5.639	0.0013	0.1235	0.0340		
		Humerus	6.134	0.0007	0.0933	0.0254		
	Grave 115	Femur	5.711	0.0008	0.1042	0.0267		
		Humerus	5.562	0.0000	0.1192	0.0282		
	Grave 136	Femur	6.220	0.0007	0.0851	0.0185		
		Humerus	5.632	0.0009	0.1171	0.0225		
	Grave 137	Femur	6.125	0.0002	0.0994	0.0226		
		Humerus	5.368	0.0001	0.1515	0.0297		
	Grave 159	Femur	5.667	0.0016	0.1416	0.0377		
		Humerus	5.592	0.0004	0.1349	0.0292		
	Grave 166	Femur	5.759	0.0010	0.0997	0.0246		
		Humerus	5.671	0.0000	0.1220	0.0258		

This equation can be used to calculate the secondary calcite content in archaeological samples:

$$[\text{calcite wt.}\%] = ([Cal/PO_4]_{ATR} + 0.0020)/0.0017 \quad (2)$$

As $v_3(CO_3)$ vibrational bands of calcite overlap with those of structural carbonate in bioapatite, thus both contributing to the determination of CO_3/PO_4, a linear correlation between CO_3/PO_4 and Cal/PO_4 (Fig. 2b) can be observed, and described by the function:

$$[CO_3/PO_4]_{ATR} = 3.5541[Cal/PO_4]_{ATR} + 0.2114 \quad (3)$$

This linear function shows that the slope is determined by the calcite content in the mixture and the intercept corresponds to the contribution of the sole carbonate contained in deproteinated bone sample. Therefore, this calibration curve can be used to obtain a correction (named CO_3/PO_4-corr) for the CO_3/PO_4 parameter, when secondary

Table 2
IRSF, Cal/PO_4 and CO_3/PO_4 calculated from ATR-FTIR and FTIR spectra of standard samples (modern deproteinated bone and calcite mixed at known percentage) and used for calibration curves.

	ATR-FTIR			FTIR		
Calcite%	IRSF	Cal/PO_4	CO_3/PO_4	IRSF	Cal/PO_4	CO_3/PO_4
20.57 (±0.01)	3.757	0.0325	0.3185	3.048	0.0301	0.7377
15.52 (±0.01)	3.774	0.0233	0.2907	3.238	0.0229	0.5557
10.46 (±0.01)	3.770	0.0162	0.2942	3.033	0.0125	0.4491
4.97 (±0.01)	4.090	0.0048	0.2183	3.253	0.0055	0.3091
2.37 (±0.01)	3.926	0.0029	0.2183	3.160	0.0020	0.2542
2.00 (±0.01)	4.085	0.0020	0.2216	–	–	–
1.50 (±0.01)	4.077	0.0002	0.2212	–	–	–
1.02 (±0.01)	3.976	0.0006	0.2135	–	–	–

calcite is detected, using the function

$$[CO_3/PO_4\text{−corr}]_{ATR} = [CO_3/PO_4]_{ATR} - 3.5541[Cal/PO_4]_{ATR} \quad (4)$$

subtracting the contribution of calcite to the 1415 cm^{-1} band by calculating the intercept of this function, once measured CO_3/PO_4 and Cal/PO_4.

4.1.2. FTIR in transmission mode

Equivalent calibration curves were obtained from the measurement of the same samples by transmission (Tr) FTIR (Fig. 2c and d, respectively; Table 2) and linear functions were similarly obtained by linear regression:

$$[\text{calcite wt.}\%] = ([Cal/PO_4]_{Tr} + 0.0024)/0.0016 \quad (5)$$

$$[CO_3/PO_4\text{−corr}]_{Tr} = [CO_3/PO_4]_{Tr} - 16.3470[Cal/PO_4]_{Tr} \quad (6)$$

4.2. ATR-FTIR spectroscopy on archaeological samples

ATR-FTIR spectra do not show any appreciable band related to the organic fraction of bones, i.e. bands at ~1660 and ~1550 cm^{-1} assigned to amide I and amide II (Fig. 1b), respectively, proving an almost complete collagen loss for all the samples, or at least a collagen content under the detection limit of this technique (~3 wt.% of collagen; Lebon et al., 2016). Therefore, Amide I/PO_4 values calculated for the four burial phases (Fig. 3a), ranging from 0.0158 to 0.0377 (Table 1), do not provide any measurement of the collagen content. This is furthermore proved by the absence of any significant trend of Amide I/PO_4 values among burial phases (Fig. 3a), as well as by the lack of any correlation between Amide I/PO_4 and IRSF (Fig. 4a) or CO_3/PO_4-corr (Fig. 4b); conversely, this was documented in other case studies for which collagen was partially preserved (Lebon et al., 2010, 2014; Reiche et al., 2010).

IRSF, which is related to bioapatite crystallinity, ranges from 4.037 to 5.218, from 4.804 to 5.202, from 4.160 to 5.805 and from 5.368 to 6.220 for pre-Mesolithic, pre-Mesolithic-b, Neolithic and Meroitic bone samples, respectively (Fig. 3b, Table 1), showing a significant variation between pre-Mesolithic bones (with the lowest IRSF values), and the Meroitic ones (with the highest IRSF values). Neolithic bones are those with a wider range of IRSF values distribution, whereas pre-Mesolithic-b ones have higher IRSF values than pre-Mesolithic bones. In any case, the IRSF values of archaeological samples are always higher than those obtained from the modern standard samples, ranging from 3.757 and 4.090.

Calcite to phosphate ratio ranges from 0.0000 to 0.0383 for pre-Mesolithic, pre-Mesolithic-b and Neolithic bones (with the exception of one Neolithic sample with Cal/PO_4 of 0.0578, corresponding to an extraordinary high calcite content), while in Meroitic bones the 712 cm^{-1} band, characteristic for calcite, was not detected and therefore Cal/PO_4 values do not exceed 0.0020 (Fig. 3c, Table 1). Calcite content for pre-Mesolithic, pre-Mesolithic-b and Neolithic samples (Fig. 3d), calculated according to the calibration curve previously established (Eq. (2)), ranges from 2.5 to 23.7 wt.%, with the exception of the previously mentioned Neolithic sample (35.2 wt.% of calcite); no significant variations were observed among burial phases. Few samples (7) have Cal/PO_4 ratio lower than 0.0020, corresponding to a calcite content lower that the detection limit, established at 2.5 wt.% (Table 1).

Carbonate to phosphate ratio ranges from 0.1584 to 0.3922, from 0.1790 to 0.2970, from 0.1117 to 0.3660 and from 0.0851 to 0.1515 for pre-Mesolithic, pre-Mesolithic-b, Neolithic and Meroitic samples, respectively (Fig. 3e, Table 1). However, it is worth to remember that this measure is affected by the occurrence of secondary calcite within the bones microstructure, since the measured 1415 cm^{-1} band results from the contribution of the $\nu_3(CO_3)$ vibrational modes of carbonate groups contained in both calcite and bioapatite. This affects all the bones with the exception of the Meroitic ones, lacking in secondary calcite. The CO_3/PO_4-corr value was calculated for all those pre-Mesolithic, pre-Mesolithic-b, Neolithic samples in which calcite was detected, using the function (4). Conversely, this correction was not applied to the few (7) samples characterised by calcite content lower that 2.5 wt.%, thus not detected, and to Meroitic bone samples; therefore CO_3/PO_4-corr values reported for these samples are equal to CO_3/PO_4 values, as calculated from infrared spectra. Corrected carbonate to phosphate ratios (CO_3/PO_4-corr) range from 0.1610 to 0.2816, from 0.1464 to 0.2145 and from 0.1024 to 0.2446 for pre-Mesolithic, pre-Mesolithic-b, Neolithic bones, respectively (Fig. 3f), being still higher than those obtained for Meroitic ones. Values ranging from 0.2014 to 0.2366 were obtained for modern standard samples used for the calibration curves.

Carbonate to phosphate ratio shows a negative correlation with IRSF ($R^2 = 0.765$) (Fig. 5a), which is furthermore improved when CO_3/PO_4-corr is considered instead of CO_3/PO_4 ($R^2 = 0.921$) (Fig. 5b). This good correlation may also indicate that the contribution of calcite, occurring in few samples but under the detection limit (2.5 wt.%), to the $\nu_3(CO_3)$ can be assumed to be minimal. Meroitic bones have higher IRSF and lower CO_3/PO_4-corr values than the pre-Mesolithic ones, while intermediated values were measured for pre-Mesolithic-b and Neolithic samples. Modern standard samples show carbonate content comparable to some of the pre-Mesolithic samples, even if IRSF values are lower. CO_3/PO_4-corr and IRSF values measured on humerus and femur of the same individual generally show a good accordance, within the accuracy of the measurement (Fig. 6). Only few cases show high intra-skeletal variability in terms of IRSF and CO_3/PO_4-corr, the most evident of which are two Neolithic graves (grave 4 and grave 158, Fig. 6c). No correlation was observed between Cal/PO_4 and CO_3/PO_4-corr (Fig. 7a), nor between Cal/PO_4 and IRSF (Fig. 7b).

Table 3
Peak positions and baselines of vibrational bands used to calculate diagenetic parameters. Baseline is defined by two points calculated as the local minimum ranging within the intervals here indicated.

Vibrational mode	Maximum peak position (cm^{-1})	Baseline (cm^{-1})
Amide I	1660	2000/1800–1400/1200
$\nu_3(CO_3)$	1415	2000/1800–1400/1201
$\nu_3(PO_4)$	1035	1400/1200–900–750
$\nu_4(CO_3)$	712	730–700
$\nu_4(PO_4)$	604	660/620–510/470
$\nu_4(PO_4)$	565	660/620–510/471

5. Discussion

5.1. Calibration curves from ATR-FTIR and Tr-FTIR spectra

Both calibration curves obtained from ATR-FTIR (Fig. 2a) and transmission FTIR (Fig. 2c) spectra show an excellent correlation and almost an equivalent trend between Cal/PO_4 and calcite percentage, thus providing an effective tool to quantify the amount of secondary calcite in archaeological bone samples. Slightly different is the situation for

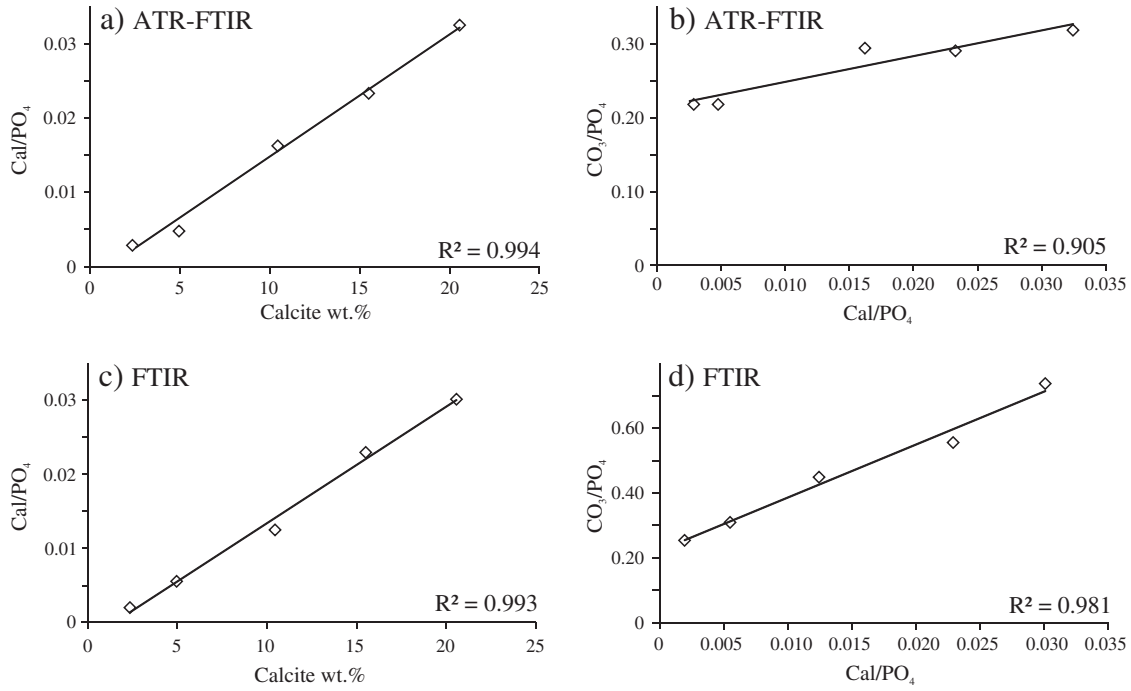

Fig. 2. Calibration curves of deproteinated bone and calcite mixtures used to quantify secondary calcite and to correct the CO_3/PO_4 parameter of archaeological bones containing secondary calcite. a. Cal/PO_4 plotted against Calcite wt.% of modern standard samples (ATR-FTIR). b. CO_3/PO_4 plotted against Cal/PO_4 of modern standard samples (ATR-FTIR). c. Cal/PO_4 plotted against Calcite wt.% of modern standard samples (FTIR). b. CO_3/PO_4 plotted against Cal/PO_4 of modern standard samples (FTIR).

calibration curves referring to the linear correlation between CO_3/PO_4 and Cal/PO_4 (Fig. 2b and d): CO_3/PO_4 ranges from 0.25 to 0.74 and from 0.21 to 0.32 for FTIR and ATR-FTIR measurements, respectively, implying a steeper slope for the FTIR calibration curve. This evidence suggests a higher sensitivity of transmission FTIR spectroscopy to the $\nu_3(CO_3)$ vibrational modes. This difference of sensitivity is typical and it is due to different physical parameters and instrumental settings underlying the two techniques and possibly related to different contributions to peak intensity from scattering and absorption effects. Nevertheless, this should not be considered a discriminating criteria for choosing one analytical technique rather than the other, at least for this type of study, since in both cases a good correlation is observed between the two parameters. The evidence that equivalent results can be obtained from ATR-FTIR and FTIR spectroscopy in transmission mode furthermore supports the choice of ATR-FTIR spectroscopy as an effective technique to investigate bone diagenesis, with the advantage of a simpler and more convenient sample preparation method.

The equations calculated from these calibration curves are not intended to be outright applicable to other studies, as the CO_3/PO_4 and Cal/PO_4 values here measured may vary, depending on the instrument or instrumental settings used for spectra acquisition. However, comparable calibration curves can be easily established for a specific instrument, according to the procedure here discussed, preparing and measuring standard samples of bone and calcite mixed at known percentage. Moreover, even if in this specific case calibration curves were obtained using deproteinated bone, chosen as a reference material for the archaeological bones from 16-D-4 site, this method can be effectively applied to other case studies. In fact, equivalent calibration curves were also obtained for mixtures of calcite and fresh bone containing collagen (data are not shown here) using the same CO_3/PO_4 and Cal/PO_4 parameters defined in this study.

5.2. Diagenetic trajectory

The previous histological and micro-morphological study on these bones (Dal Sasso et al., 2014), focused on the investigation of bone diagenesis at the micro-scale level, pointed out the occurrence of alteration patterns due to microbial activity, secondary mineral phases precipitation and dissolution. All these features were related to local burial and environmental conditions, compatibly with data obtained from archaeological and geomorphological investigations at Al Khiday (Cremaschi et al., 2007; Salvatori et al., 2011; Williams et al., 2015; Zerboni, 2011) and with the palaeoenvironmental reconstruction at regional level (Clarke et al., 2015; Gasse, 2000; Gatto and Zerboni, 2015; Nicoll, 2004; Williams, 2009; Williams and Jacobsen, 2011; Williams et al., 2015; Zerboni, 2013). Pre-Mesolithic and pre-Mesolithic-b bones experienced a more humid burial environment with respect to the subsequent burial phases, in accordance with palaeoenvironmental records that indicate higher water availability, due to a more intense monsoonal activity, leading to higher flooding levels of the White Nile and to the formation of seasonal swamps in the area. By middle Holocene, at the time of the Neolithic burial phase, climate gradually changed towards drier conditions characterised by a weaker monsoonal activity and by the progressive decrease of rainfall and water availability. By the Meroitic period, and later on, a more arid climate was established, and bones, consequently, underwent diagenetic processes typical of arid or semi-arid environment.

Collagen preservation strictly depends on climatic and burial conditions, in particular on temperature and pH of soil solutions (Collins et al., 2002; Hedges et al., 1995; Smith et al., 2007). Collagen loss can be caused by chemical hydrolysis, alteration of the bone mineral fraction and/or microbial degradation (Collins et al., 2002). Chemical hydrolysis is particularly effective when high temperature and extremes pH values (alkaline in particular) occur in the burial environment. Microbial activity, detected by characteristic alteration patterns described as non-Wedl microscopic focal destruction (non-Wedl MFD) by Hackett (1981), is responsible for the dissolution and reprecipitation of bioapatite; this leads to the exposure of collagen to pore solutions and to microbial enzymes causing its subsequent degradation. Collagen exposure to pore fluids can also be related to bioapatite recrystallization. In this case study, collagen loss was observed for all burial phases, whereas the microbial activity was detected only in pre-Mesolithic, pre-Mesolithic-b and

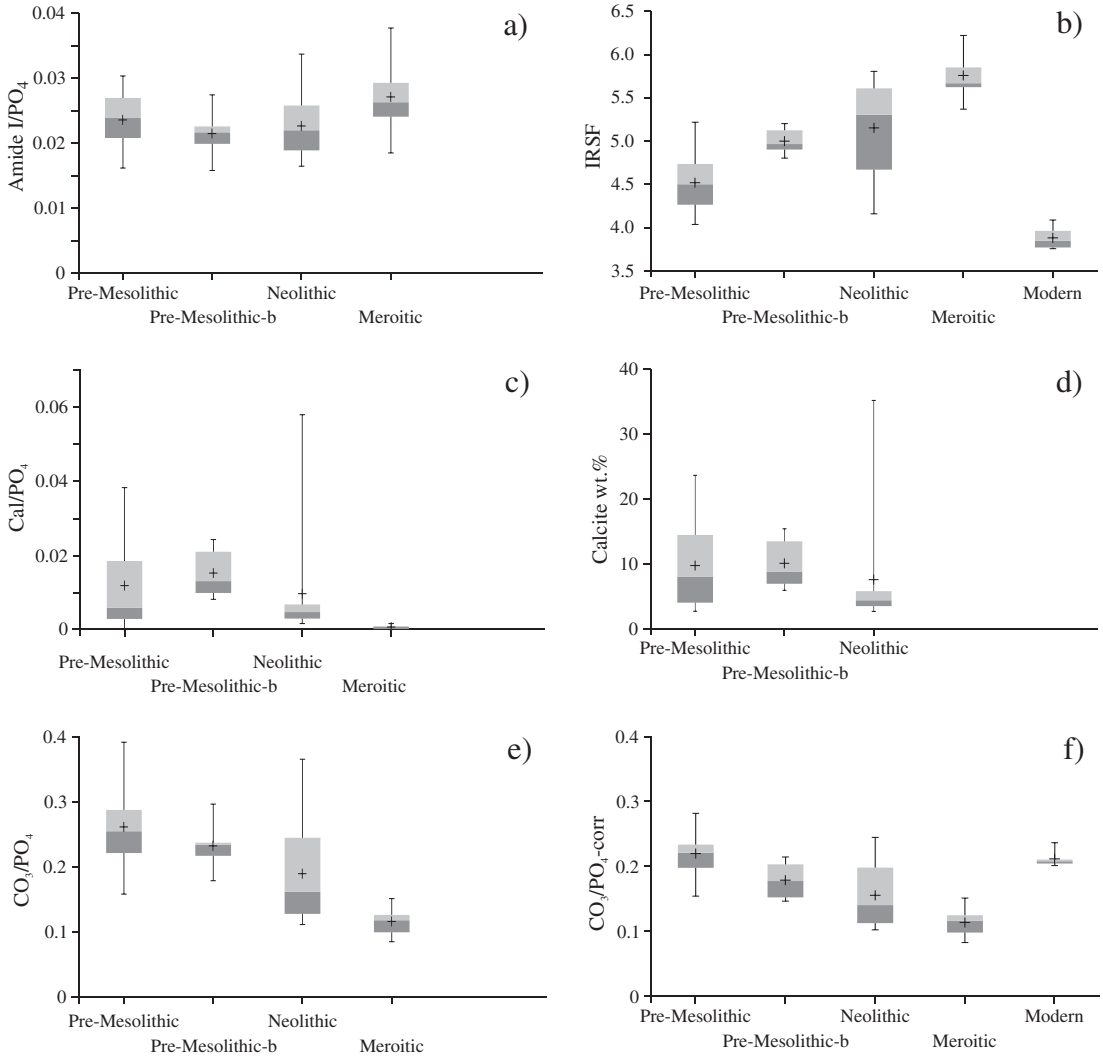

Fig. 3. Box plot of the frequency distribution of diagenetic parameters calculated from ATR-FTIR spectra of pre-Mesolithic, pre-Mesolithic-b, Neolithic and Meroitic bone samples: a. Collagen content parameter: Amide I/PO_4; b. Infrared splitting factor: IRSF; c. Parameter related to the secondary calcite content: Cal/PO_4; d. Secondary calcite percentage: Calcite wt.%; e. Parameter related to the content of the structural carbonate of bioapatite CO_3/PO_4; f. Correction of CO_3/PO_4 taking into account the contribution of calcite to the $\nu_3(CO_3)$ vibrational mode: CO_3/PO_4-corr.

Neolithic bones, being totally absent in the Meroitic ones. Therefore, a combined contribution of both chemical hydrolysis and microbial attack may have been responsible for the collagen loss in the bones from the Al Khiday site. In turn, collagen loss may play a significant role in bioapatite recrystallization, as nanocrystals turn out to be exposed to the burial environment, thus being more susceptible to alteration (Collins et al., 2002).

Archaeological bones usually have higher IRSF values than modern ones due to diagenetic alteration. Bioapatite nanocrystals tend to recrystallize (presumably by Ostwald ripening process; Ostwald, 1897) into a more thermodynamically stable structure, implying a more ordered crystal structure, a larger crystal size and therefore a significant reduction of the specific surface area (Hedges et al., 1995; Nielsen-Marsh and Hedges, 2000). In this case study, recrystallization degree of bones

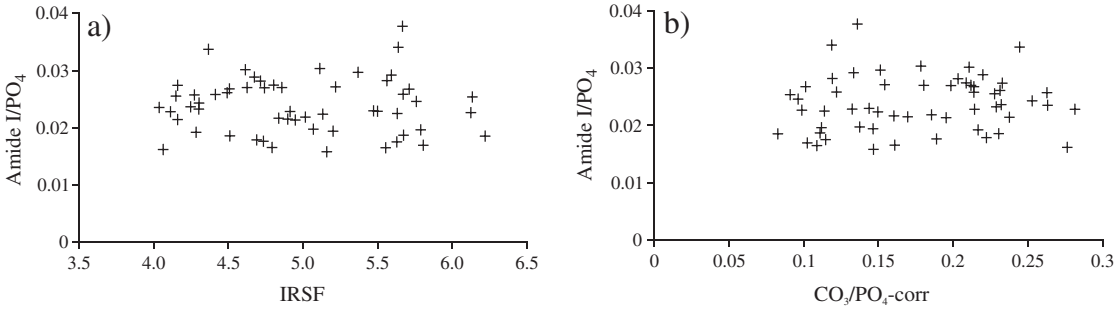

Fig. 4. a. Amide I/PO_4 plotted against IRSF and b. Amide I/PO_4 plotted against CO_3/PO_4-corr of archaeological bone samples (ATR-FTIR).

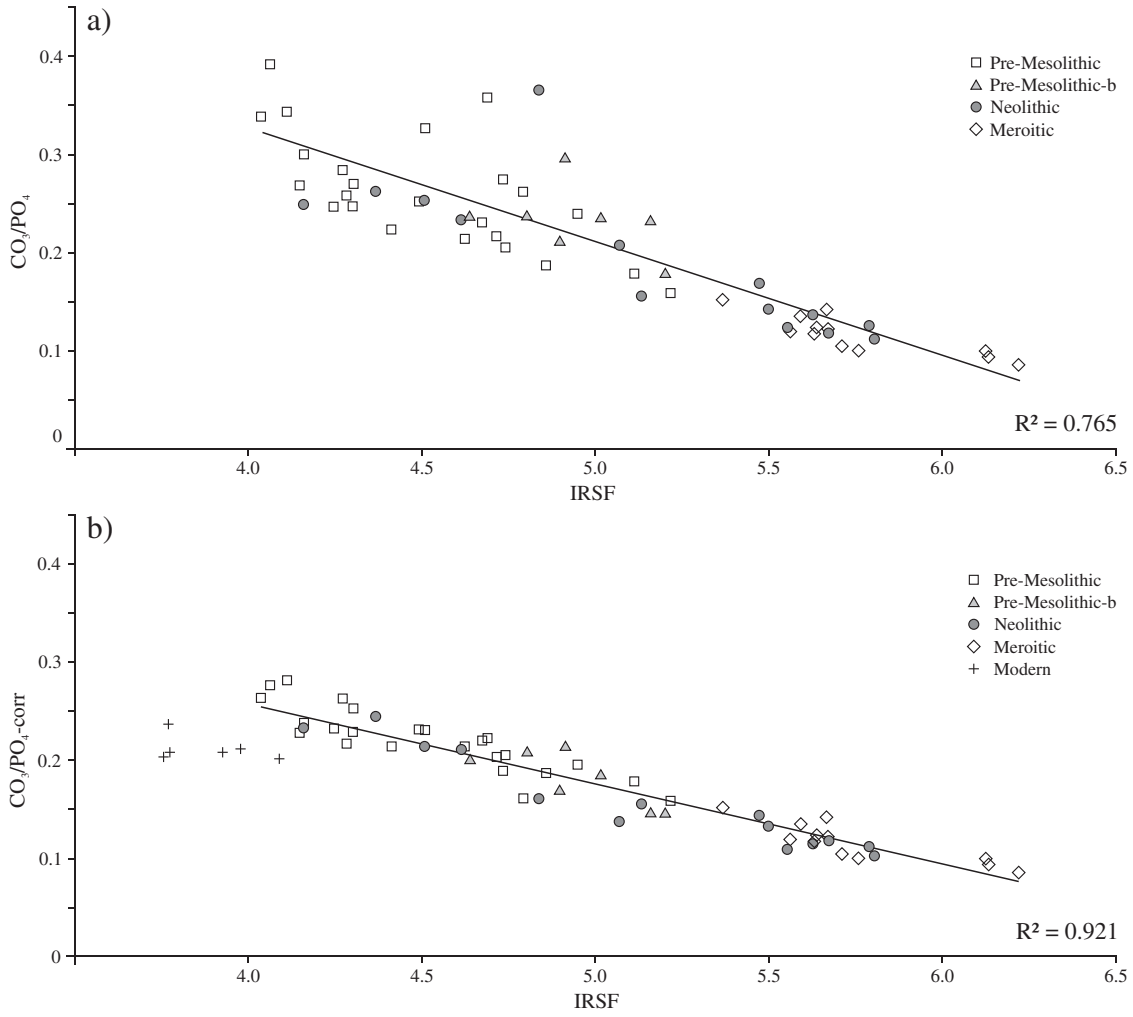

Fig. 5. a. CO_3/PO_4 plotted against IRSF of archaeological bone samples among the different burial phases (ATR-FTIR); b. CO_3/PO_4-corr plotted against IRSF of archaeological bone samples among burial phases (ATR-FTIR); parameters obtained from modern samples (used for the calibration curves), are shown as reference.

can be monitored by the correlation between crystallinity parameter (IRSF) and carbonate content (CO_3/PO_4-corr) (Fig. 5b), where higher IRSF values and lower carbonate content identify the more recrystallized bones. Interesting to note is that the recrystallization process differently behaved among burial phases as Meroitic bones result to be the most altered, whereas the pre-Mesolithic ones show IRSF and CO_3/PO_4-corr values closer to those of modern bones. These observations suggest that recrystallization process is more influenced by burial and environmental conditions rather than by the age of the burial. In fact, assuming the degree of recrystallization to be proportional with time, without considering the changes of burial conditions, could lead to misleading conclusions. Moreover, these results show that the environmental conditions occurring in the last two millennia differently affected bones of the Meroitic phase with respect to those of the more ancient burials, which were already altered by several diagenetic processes occurred in the previous millennia. Different local pH conditions in the burial environment may also be responsible for these differences observed among burial phases. According to the diachronic sequence of diagenetic events (Dal Sasso et al., 2014) defined on the basis of textural relationships between different types of diagenetic alterations, pre-Mesolithic, pre-Mesolithic-b and Neolithic burials suffered first of microbial attack, presumably shortly after burial; then secondary calcite precipitated as a consequence of changes in the soil evapotranspiration conditions during the alternation of wet and dry periods, which punctuated the early and middle Holocene. Therefore, the precipitation of secondary calcite, meaning an alkaline burial environment, at a certain point of the diagenetic history of these bones may be responsible for a low recrystallization rate for bioapatite, according to the model proposed by Berna et al. (2004). Despite the occurrence of pedogenic calcium-carbonate-rich horizons at Al Khiday site (Zerboni, 2011), the complete absence of secondary calcite in Meroitic bones suggests a limited circulation of water within the sediments since bones deposition, in accordance with the drier climatic conditions in which they were buried; therefore the local burial environment was possibly less alkaline than that experienced by bones of the previous burial phases. This would have determined an increase in the recrystallization rate (Berna et al., 2004) in the Meroitic bones. Despite these considerations, neither correlations between the actual content of secondary calcite (determined by Cal/PO_4) and CO_3/PO_4-corr (Fig. 7a) or IRSF (Fig. 7b), nor appreciable differences in secondary calcite content among pre-Mesolithic, pre-Mesolithic-b and Neolithic burial phases are observed (Fig. 3d), thus suggesting that recrystallization processes are more influenced by the presence or absence of secondary calcite rather than by its amount (Fig. 7b).

On the basis of the distribution of IRSF and CO_3/PO_4-corr values (Fig. 5b), despite being highly variable, pre-Mesolithic and Meroitic bone samples are well distinguishable in two groups, while pre-Mesolithic-b and Neolithic ones are spread within intermediate values. When the

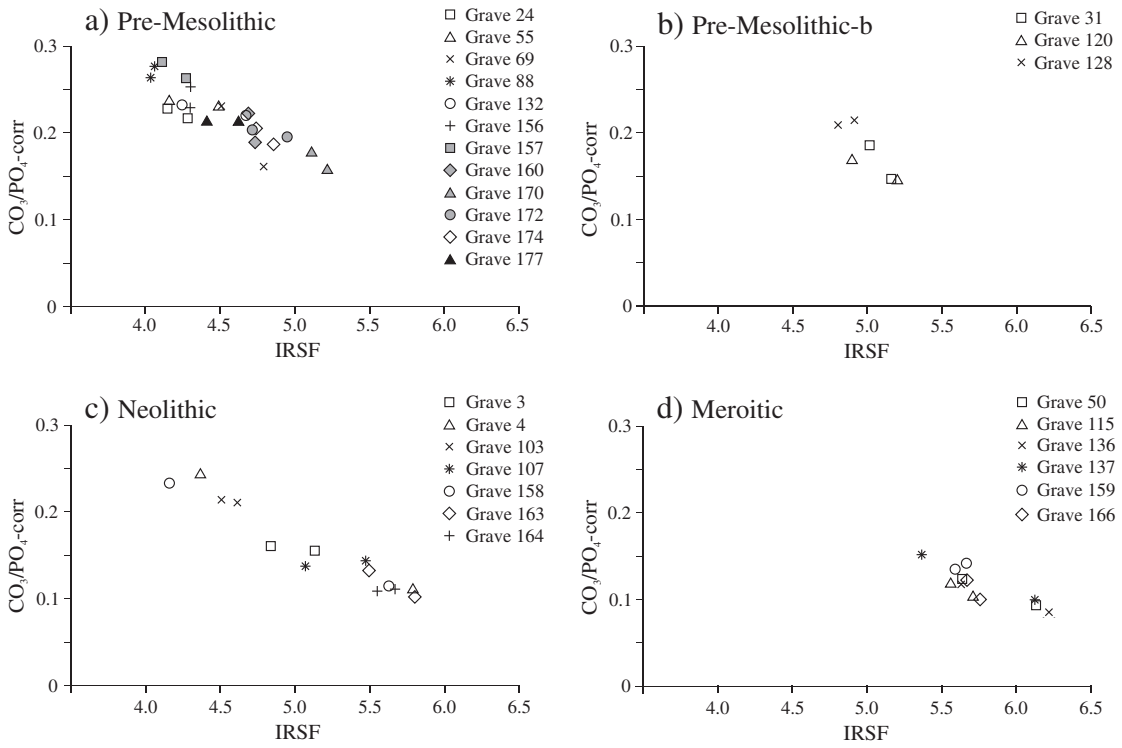

Fig. 6. a. CO_3/PO_4-corr plotted against IRSF of pre-Mesolithic bone samples (ATR-FTIR); b. CO_3/PO_4-corr plotted against IRSF of pre-Mesolithic-b bone samples (ATR-FTIR); c. CO_3/PO_4-corr plotted against IRSF of Neolithic bone samples (ATR-FTIR); d. CO_3/PO_4-corr plotted against IRSF of Meroitic bone samples (ATR-FTIR).

distribution of these values is considered within each burial phase (Fig. 6), a good accordance of IRSF and CO_3/PO_4-corr values obtained on humerus and femur of the same individual can be observed (with few exceptions, such as Neolithic graves 4 and 158). High variability within a single burial phase may be due to changes in local burial conditions; this may also explain those few cases of high intra-skeletal variability, supposing particularly localised changes in burial conditions.

6. Conclusions

This case study shows the effects of diagenetic processes along a wide chronological period covering almost the entire Holocene, and in particular describes the variability of diagenetic alteration of bones due to climatic changes. These results, obtained from an extensive FTIR spectroscopy investigation, suggest that differences in diagenetic alteration observed between several burial phases are directly influenced by palaeoenvironmental conditions and climatic changes occurring at regional level. Moreover, variations of local burial conditions may contribute to increase the variability of bones alteration state within a single burial phase.

The number of diagenetic parameters that can be obtained from FTIR spectra provides valuable information on chemical and structural alteration of bone material. Moreover, under a methodological viewpoint, ATR-FTIR spectroscopy, even if occasionally applied, results to be a convenient technique in the diagenetic study of bones, with the advantages of a minimal sample preparation and faster analytical procedure with respect to the transmission mode. Considering the inexpensive and fast analytical procedure and the low amount of required material, the micro-invasive ATR-FTIR measurements can be performed on a large set of samples; this enables one to acquire detailed and statistically significant information on the bones preservation state as well as on the diagenetic processes involved. Moreover, ATR-FTIR spectroscopy can be effectively applied as a screening method on large sets of samples in order to select the better preserved bones potentially suitable for subsequent analyses. Since both the degree of alteration and the occurrence of secondary phases can influence the recovery of information regarding the pristine composition of bone material, ATR-FTIR spectroscopy

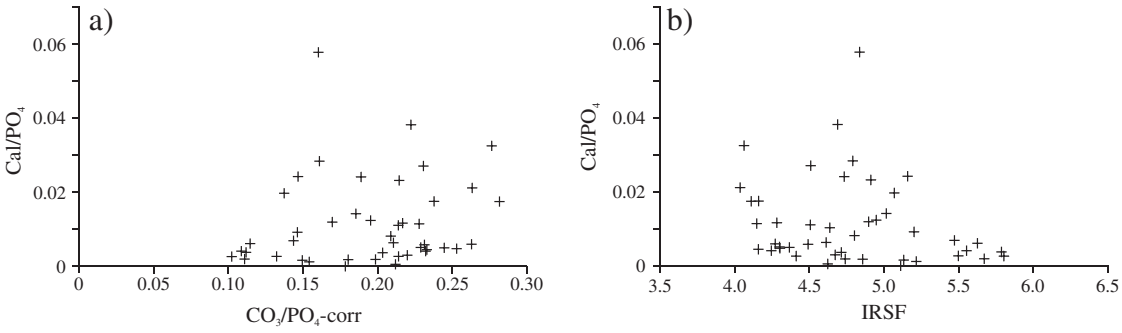

Fig. 7. a. Cal/PO_4 plotted against CO_3/PO_4-corr and b. Cal/PO_4 plotted against IRSF of archaeological bone samples (ATR-FTIR).

can suggest the more promising samples that could provide reliable results with further analyses.

Acknowledgements

We are grateful to Sandro Salvatori, co-director of "El Salha Archaeological Project" for the precious collaboration. We would like to thank Tina Jakob for her help for bone sampling. We thank the Italian Ministry of Foreign Affairs (DGSP) and Centro Studi Sudanesi e sub-Sahariani (CSSeS) for funding the archaeological research; we kindly thank the National Corporation for Antiquities and Museums (Khartoum, Sudan) for authorising the study of archaeological bones and the Italian Embassy in Khartoum for the support. We would like to thank two anonymous reviewers for their critical reading and suggestions that improved the quality of this manuscript.

Appendix A. Supplementary data

Supplementary data associated with this article can be found in the online version, at http://dx.doi.org/10.1016/j.palaeo.2016.10.005. These data include the Google map of the most important areas described in this article.

References

Asscher, Y., Weiner, S., Boaretto, E., 2011a. Variations in atomic disorder in biogenic carbonate hydroxyapatite using the infrared spectrum grinding curve method. Adv. Funct. Mater. XX, 1–6.

Asscher, Y., Regev, L., Weiner, S., Boaretto, E., 2011b. Atomic disorder in fossil tooth and bone mineral: an FTIR study using the grinding curve method. Archaeoscience 35, 135–141.

Beasley, M.M., Bartelink, E.J., Taylor, L., Miller, R.M., 2014. Comparison of transmission FTIR, ATR, and DRIFT spectra: implications for assessment of bone bioapatite diagenesis. J. Archaeol. Sci. 46, 16–22.

Berna, F., Matthews, A., Weiner, S., 2004. Solubilities of bone mineral from archaeological sites: the recrystallization window. J. Archaeol. Sci. 31 (7), 867–882.

Castaneda, I.S., Mulitza, S., Schefuß, E., Lopes dos Santos, R.A., Sinninghe Damsté, J.S., Schouten, S., 2009. Wet phases in the Sahara/Sahel region and human migration patterns in North Africa. PNAS 106 (48), 20159–20163.

Clarke, J., Brooks, N., Banning, E.B., Bar-Matthews, M., Campbell, S., Clare, L., Cremaschi, M., di Lernia, S., Drake, N., Gallinaro, M., Manning, S., Nicoll, K., Philip, G., Rosen, S., Schoop, U.-D., Tafuri, M.A., Weninger, B., Zerboni, A., 2015. Climatic changes and social transformations in the Near East and North Africa during the 'long' 4th millennium BC: a comparative study of environmental and archaeological evidence. Quat. Sci. Rev. 136, 96–121.

Collins, M.J., Nielsen-Marsh, C.M., Hiller, J., Smith, C.I., Roberts, J.P., Prigodich, R.V., Weiss, T.J., Csapo, J., Millard, A.R., Turner-Walker, G., 2002. The survival of organic matter in bone: a review. Archaeometry 44 (3), 383–394.

Cremaschi, M., Salvatori, S., Usai, D., Zerboni, A., 2007. A further tessera to the huge mosaic: studying the ancient settlement pattern of the El Salha region (south-west of Omdurman, Central Sudan). In: Kroeper, K., Chlodnicki, M., Kobusiewicz, M. (Eds.), Archaeology of the Earliest North-eastern Africa. Poznan Archaeological Museum, pp. 39–48.

Dal Sasso, G., Maritan, L., Usai, D., Angelini, I., Artioli, G., 2014. Bone diagenesis at the micro-scale: bone alteration patterns during multiple burial phases at Al Khiday (Khartoum, Sudan) between the Early Holocene and the II century AD. Palaeogeogr. Palaeoclimatol. Palaeoecol. 416, 30–42.

Elliot, J.C., 2002. In: Kohn, M.J., Rakovan, J., Hughes, J.M. (Eds.), Calcium Phosphate Biominerals. Phosphates: Geochemical, Geobiological and Materials Importance. Reviews in Mineralogy and Geochemistry 48, pp. 427–453.

Gasse, F., 2000. Hydrological changes in the African tropics since the Last Glacial Maximum. Quat. Sci. Rev. 19, 189–211.

Gatto, M.C., Zerboni, A., 2015. Holocene supra-regional environmental changes as trigger for major socio-cultural processes in northeastern Africa and the Sahara. Afr. Archaeol. Rev. 32 (2), 301–333.

Gómez-Morales, J., Iafisco, M., Delgado-López, J.M., Sarda, S., Drouet, C., 2013. Progress in the preparation of nanocrystalline apatites and surface characterization: overview of fundamental and applied aspects. Prog. Cryst. Growth Charact. Mater. 59, 1–46.

Grunenwald, A., Keyser, C., Sautereau, A.M., Crubézy, E., Ludes, B., Drouet, C., 2014. Revisiting carbonate quantification in apatite (bio)minerals: a validated FTIR methodology. J. Archaeol. Sci. 49, 134–141.

Hackett, C.J., 1981. Microscopical focal destruction (tunnels) in excavated human bones. Med. Sci. Law 21, 243–265.

Hedges, R.E.M., 2002. Bone diagenesis: an overview of the processes. Archaeometry 44 (3), 319–328.

Hedges, R.E.M., Millard, A.R., Pike, A.W.G., 1995. Measurements and relationships of diagenetic alteration of bone from three archaeological sites. J. Archaeol. Sci. 22, 201–209.

Hoelzmann, P., Keding, B., Berke, H., Kröpelin, S., Kruse, H.J., 2001. Environmental change and archaeology: lake evolution and human occupation in the Eastern Sahara during the Holocene. Palaeogeogr. Palaeoclimatol. Palaeoecol. 169 (3), 193–217.

Hollund, H.I., Ariese, F., Fernandes, R., Jans, M.M.E., Kars, H., 2012. Testing an alternative high throughput tool for investigating bone diagenesis: FTIR in attenuated total reflection (ATR) mode. Archaeometry 55 (3), 507–532.

Iacumin, P., Di Matteo, A., Usai, D., Salvatori, S., Venturelli, G., 2016. Stable isotope study on ancient populations of Central Sudan: insights on their diet and environment. Am. J. Phys. Anthropol. http://dx.doi.org/10.1002/ajpa.22987 (in press).

Jakob, T., 2014. A Bioarchaeological Appraisal of the Human Skeletal Remains from e l-Khiday 2, Central Sudan. In: Anderson, J.R., Welsby, D.A. (Eds.), The Fourth Cataract and Beyond. Proceedings of the 12th International Conference for Nubian Studies. Peeters, Leuven, pp. 271–277.

Kröpelin, S., Verschuren, D., Lézine, A.M., Eggermont, H., Cocquyt, C., Francus, P., Cazet, J.P., Fagot, M., Rumes, B., Russell, J.M., Darius, F., Conley, D.J., Schuter, M., von Suchodoletz, H., Engstrom, D.R., 2008. Climate-driven ecosystem succession in the Sahara: the past 6000 years. Science 320, 765–768.

Lebon, M., Reiche, I., Fröhlich, F., Bahain, J.J., Falguères, C., 2008. Characterization of archaeological burnt bones: contribution of a new analytical protocol based on derivative FTIR spectroscopy and curve fitting of the ν 1 ν 3 PO4 domain. Anal. Bioanal. Chem. 392 (7–8), 1479–1488.

Lebon, M., Reiche, I., Bahain, J.-J., Chadefaux, C., Moigne, A.-M., Fröhlich, F., Sémah, F., Schwarcz, H.P., Falguères, C., 2010. New parameters for the characterization of diagenetic alterations and heat-induced changes of fossil bone mineral using Fourier Transform Infrared Spectrometry. J. Archaeol. Sci. 37, 2265–2276.

Lebon, M., Zazzo, A., Reiche, I., 2014. Screening in situ bone and teeth preservation by ATR-FTIR mapping. Palaeogeogr. Palaeoclimatol. Palaeoecol. 416, 110–119.

Lebon, M., Reiche, I., Gallet, X., Bellot-Gurlet, L., Zazzo, A., 2016. Rapid quantification of bone collagen content by ATR-FTIR spectroscopy. Radiocarbon 58 (1), 131–145.

Lee-Thorp, J.A., 2008. On isotopes and old bones. Archaeometry 50 (6), 925–950.

LeGeros, R.Z., 1981. Apatites in biological systems. Prog. Cryst. Growth Charact. Mater. 4, 1–45.

Nicoll, K., 2004. Recent environmental changes and prehistoric human activity in Egypt and Northern Sudan. Quat. Sci. Rev. 23, 564–580.

Nielsen-Marsh, C.M., Hedges, R.E.M., 2000. Patterns of diagenesis in bone I: the effects of site environments. J. Archaeol. Sci. 27, 1139–1150.

Ostwald, W., 1897. Studien über die Bildung und Umwandlung fester Körper. Z. Phys. Chem. 22, 289–330.

Piga, G., Santos-Cubedo, A., Brunetti, A., Piccinini, M., Malgosa, A., Napolitano, E., Enzo, S., 2011. A multi-technique approach by XRD, XRF, FT-IR to characterize the diagenesis of dinosaur bones from Spain. Palaeogeogr. Palaeoclimatol. Palaeoecol. 310, 92–107.

Reiche, I., Lebon, M., Chadefaux, C., Müller, K., Le Hô, A., Gensch, M., Schade, U., 2010. Microscale imaging of the preservation state of 5,000-year-old archaeological bones by synchrotron infrared microspectroscopy. Anal. Bioanal. Chem. 397, 2491–2499.

Rey, C., Combes, C., Drouet, C., Grossin, D., 2011. Bioactive ceramics: physical chemistry. In: Ducheyne, P., Healy, K.E., Hutmacher, D.W., Grainger, D.W., Kirkpatrick, C.J. (Eds.), Comprehensive Biomaterials, 1. Elsevier, pp. 187–221.

Rink, W.J., Schwarcz, H.P., 1995. Tests for diagenesis in tooth enamel: ESR dating signals and carbonate contents. J. Archaeol. Sci. 22 (2), 251–255.

Roche, D., Ségalen, L., Balan, E., Delattre, S., 2010. Preservation assessment of Miocene–Pliocene tooth enamel from Tugen Hills (Kenyan Rift Valley) through FTIR, chemical and stable-isotope analyses. J. Archaeol. Sci. 37, 1690–1699.

Salesse, K., Dufour, E., Lebon, M., Wurster, C., Castex, D., Bruzek, J., Zazzo, A., 2014. Variability of bone preservation in a confined environment: the case of the catacomb of Sts Peter and Marcellinus (Rome, Italy). Palaeogeogr. Palaeoclimatol. Palaeoecol. 416, 43–54.

Salvatori, S., 2012. Disclosing archaeological complexity of the Khartoum Mesolithic. New data at the site and regional level. Afr. Archaeol. Rev. 29, 399–472.

Salvatori, S., Usai, D., 2009. El Salha Project 2005: new Khartoum Mesolithic sites from central Sudan. Kush 19, 87–96.

Salvatori, S., Usai, D., Zerboni, A., 2011. Mesolithic site formation and palaeoenvironment along the White Nile (Central Sudan). Afr. Archaeol. Rev. 28, 177–211.

Salvatori, S., Usai, D., Faroug, M.A., Di Matteo, A., Iacumin, P., Lindseele, V., Magzoub, M.K., 2014. Archaeology at Al Khiday: new insight on the prehistory and history of Central Sudan. In: Anderson, J.R., Welsby, D.A. (Eds.), The Fourth Cataract and Beyond. Proceedings of the 12th International Conference of Nubian Studies. Peeters, Leuven, pp. 243–247.

Smith, C.I., Nielsen-Marsh, C.M., Jans, M.M.E., Collins, M.J., 2007. Bone diagenesis in the European Holocene I: patterns and mechanisms. J. Archaeol. Sci. 34, 1485–1493.

Sponheimer, M., Lee-Thorp, J.A., 1999. Alteration of enamel carbonate environments during fossilization. J. Archaeol. Sci. 26, 143–150.

Stathopoulou, E.T., Psycharis, V., Chryssikos, G.D., Gionis, V., Theodorou, G., 2008. Bone diagenesis: new data from infrared spectroscopy and X-ray diffraction. Palaeogeogr. Palaeoclimatol. Palaeoecol. 266, 168–174.

Surovell, T.A., Stiner, M.C., 2001. Standardizing infra-red measures of bone mineral crystallinity: an experimental approach. J. Archaeol. Sci. 28, 633–642.

Talbot, M.R., Filippi, M.L., Jensen, N.B., Tiercelin, J.J., 2007. An abrupt change in the African monsoon at the end of the Younger Dryas. Geochem. Geophys. Geosyst. 8 (3). http://dx.doi.org/10.1029/2006GC001465.

Trueman, C.N.G., Behrensmeyer, A.K., Tuross, N., Weiner, S., 2004. Mineralogical and compositional changes in bones exposed on soil surface in Amboseli National Park, Kenya: diagenetic mechanisms and the role of sediment pore fluids. J. Archaeol. Sci. 31, 721–739.

Usai, D., Salvatori, S., 2005. The IsIAO archaeological project in the El Salha area (Omdurman South, Sudan): results and perspectives. Africa 60 (3–4), 474–493.

Usai, D., Salvatori, S., 2007. The oldest representation of a Nile boat. Antiquity 81, 314.

Usai, D., Salvatori, S., Iacumin, P., Di Matteo, A., Jakob, T., Zerboni, A., 2010. Excavating a unique pre-Mesolithic cemetery in Central Sudan. Antiquity 84, 323.
Usai, D., Salvatori, S., Jakob, T., David, R., 2014. The Al Khiday cemetery in Central Sudan and its "Classic/Late Meroitic" period graves. Journal of African Archaeology 12 (2), 183–204.
Weiner, S., 2010. Biological materials: bones and teeth. In: Weiner, S. (Ed.), Microarchaeology: Beyond the Visible Archaeological Record. Cambridge University press, pp. 99–134.
Weiner, S., Bar-Yosef, O., 1990. State of preservation of bones from prehistoric sites in the Near East: a survey. J. Archaeol. Sci. 17, 187–196.
Weiner, S., Wagner, H.D., 1998. The material bone: structure-mechanical function relations. Annu. Rev. Mater. Sci. 28, 271–298.
Williams, M.A.J., 2009. Late Pleistocene and Holocene environments in the Nile basin. Glob. Planet. Chang. 69, 1–15.
Williams, M.A.J., Jacobsen, G.E., 2011. A wetter climate in the desert of northern Sudan 9900–7600 years ago. Sahara 22, 7–14.
Williams, M.A.J., Donatella, U., Salvatori, S., Williams, F.M., Zerboni, A., Maritan, L., Linseele, V., 2015. Late Quaternary environments and prehistoric occupation in the lower White Nile valley, central Sudan. Quat. Sci. Rev. 130, 72–88.
Wopenka, B., Pasteris, J.D., 2005. A mineralogical perspective on the apatite in bone. Mater. Sci. Eng. 25 (2), 131–143.
Zerboni, A., 2011. Micromorphology reveals in situ Mesolithic living floors and archaeological features in multiphase sites in Central Sudan. Geoarchaeology: An International Journal 26, 365–391.
Zerboni, A., 2013. In: Shirai, N. (Ed.), Early Holocene Palaeoclimate in North Africa: An Overview. Neolithisation of Northeastern Africa, Studies in Early Near Eastern Production, Subsistence, and Environment, Berlin, ex oriente 16, pp. 65–82.